energies

MDPI

Article

A Non-Equilibrium Thermodynamic Approach for Analysis of Power Conversion Efficiency in the Wind Energy System

Ihor Shchur [1,*], Marek Lis [2,*] and Yurii Biletskyi [1]

[1] Department of Electric Mechatronics and Computer-Controlled Electromechanical Systems, Lviv Polytechnic National University, 79013 Lviv, Ukraine; yurii.o.biletskyi@lpnu.ua
[2] Faculty of Electrical Engineering, Czestochowa University of Technology, 35-959 Czestochowa, Poland
* Correspondence: ihor.z.shchur@lpnu.ua (I.S.); marek.lis@pcz.pl (M.L.); Tel.: +38-097-5951298 (I.S.); +48-602344809 (M.L.)

Abstract: This article proposes an approach and develops an appropriate method of applying linear non-equilibrium thermodynamics to analyze energy processes, in particular using the example of the wind energy conversion system (WECS) with a directly connected vertical axis wind turbine (VAWT) and vector-controlled permanent magnet synchronous generator (PMSG). The main steps of the proposed approach are the description of the component subsystems as universal linear or linearized energy converters (ECs), which are characterized by several dimensionless parameters, the main one of which is the degree of coupling between their input and output. According to their value, as well as justified efficiency criteria, the optimal operating points of each ECs can be easily found. Such an approach makes it possible to abstract from physical laws of a different nature and equally assess the work of each of the subsystems. The next step is a connection of the received ECs. As shown in the paper, for the most common cascade connection of ECs, there are the best conditions for their connection, under which the newly formed equivalent EC can have maximum efficiency. This opens up an opportunity to analyze the influence of already real parameters of cascaded interconnected subsystems on the quality of their connection and justify specific solutions that would not have been seen without this approach. For example, in this study, from all parameters of the PMSG, only the selection of the optimal rated inductance of the armature winding made it possible to improve the quality of the connection of the PMSG with a specific VAWT and approximate the efficiency of the entire WECS to the maximum possible, especially in medium and high winds.

Keywords: non-equilibrium; thermodynamics; energy processes; wind energy conversion system (WECS); vertical axis wind turbine (VAWT); permanent magnet synchronous generator (PMSG); cascade connection

Citation: Shchur, I.; Lis, M.; Biletskyi, Y. A Non-Equilibrium Thermodynamic Approach for Analysis of Power Conversion Efficiency in the Wind Energy System. *Energies* **2023**, *16*, 5234. https://doi.org/10.3390/en16135234

Academic Editor: Annunziata D'Orazio

Received: 7 June 2023
Revised: 28 June 2023
Accepted: 5 July 2023
Published: 7 July 2023

1. Introduction

The efficiency of energy conversion is a crucial factor in achieving energy savings within various industries' technological processes. While renewable energy utilizes natural and freely available energy sources, enhancing the efficiency of energy transformation in renewable energy systems contributes to increased power generation at specific equipment capacities and helps reduce the cost of the obtained energy.

The analysis of energy efficiency in various systems relies on the fundamental science of thermodynamics. Initially, during its early development in the first half of the 19th century, initiated by the work of Sadi Carnot, thermodynamics primarily focused on describing reversible processes and isolated systems with the significant presence of thermal energy. The name of the science itself, "thermodynamics," reflects this emphasis on thermal energy. Classical thermodynamics, developed by Rudolf Clausius in the latter half of the 19th century, played a pivotal role in establishing a fundamental science that enables the analysis of energy transformations in reversible processes. Clausius's approach, based on a phenomenological macroscopic description of systems encompassing diverse physical and

later chemical phenomena, provided a framework for studying energy transformations without considering the specific timing of their occurrence [1]. This makes it possible to outline the thermodynamic limits of process efficiency, which has not lost its relevance to this day. Linear non-equilibrium thermodynamics, which was developed from classical thermodynamics in the middle of the 20th century thanks to the works of Lars Onsager, summarized the general theoretical foundations for the energy regularities of not only isolated, but also closed and open systems with real irreversible processes, taking into account their flow speed. As a result, a clear mathematical apparatus was developed, especially for linear systems, which allows for the unification and description of energy transformations [2]. Thermodynamics found its further development in the works of F. Curzon and B. Ahlborn on modeling real systems by combining reversible and irreversible subsystems. This section of thermodynamics was named endoreversible thermodynamics [3]. It makes it possible to establish relationships between efficiency and power output, which is especially important for the study of natural biochemical processes. Currently, due to its fundamental nature, thermodynamics is used to describe energy transformations in all types of systems of various natures—physical, chemical, biological—and is even used to study regularities in informational, social systems, etc. Its comprehensiveness can be judged from the work [4], where all natural and anthropogenic processes taking place on planet Earth are subjected to thermodynamic analysis.

Renewable energy, which combines systems of different natures, between which energy exchange and energy transformation take place, has recently become an object of thermodynamics research. This also applies to wind energy [5], where the energy of the wind flow (aerodynamic subsystem) is transformed into the mechanical energy of the wind turbine (WT) and then, through an electromechanical transformation in the generator and electrical transformation in the power electronic system controlling its operation, into electrical energy. Most research on WTs is aimed at improving their effectiveness. As for small WTs, the search for new efficient configurations, which would be easy to start up and work productively in conditions with small and rapidly changing wind speeds, is constantly ongoing [6]. For high-capacity WTs, which are typically installed in conditions characterized by high and stable wind speeds, the configurations of the WTs themselves are already well established. However, there are new problems associated with the organization of wind farms, for example, wind farm arrangements, variations in WT capacities, effective control in different wind ranges [7], production interactions in the substantial offshore wind farms [8], increasing the reliability of work under specific operating conditions, and reductions of acoustic noise, in particular, the control of WTs according to the noise and power trade-offs graphics [9]. Although the vast majority of research in wind energy is devoted to many of its other important problems, thermodynamic analysis is already used in new works, and energy and exergy terminology is introduced [10]. For example, in [11], the comparison of the impacts on WT efficiencies of four meteorological variables, such as wind speed, pressure, temperature, and the humidity ratio was investigated. As a result of research, it was shown that although wind speed dominates the turbine's efficiency performance, other meteorological variables also play important roles. More complex multi-generation hybrid renewable energy systems are also possible [12], with the further conversion of renewable energy in storage systems, for example, in the potential energy of compressed air [13], production of hydrogen or ammonia [14], novel combined cooling, heating systems using wind energy [15], and complex systems with a combination of different methods of energy generation and accumulation [16]. In similar works, thermodynamic analysis is used to assess the quality of energy and its exergy and search for optimal solutions [17].

Such studies analyze the flow of energy or exergy and its transformation in the specific subsystems of the WT, multiplicator, and generator, but do not determine ways to increase the energy efficiency of the entire wind energy conversion system (WECS). To identify the latter, a more detailed analysis is required, which is based on a mathematical description of the processes in the WECS components. However, a detailed description of interconnected

processes of different physical natures that take place in WECS components—aerodynamic, mechanical, electromagnetic—complicates the understanding and does not reveal all the problems associated with a decrease in energy efficiency. An effective approach to solving the problem of increasing WECS efficiency can be the application of methods of linear thermodynamics of non-equilibrium processes, which made it possible to successfully solve many complex problems, especially with coupled effects. A feature of the linear thermodynamics of non-equilibrium processes is the ability to describe complex, including non-linear steady-state processes of various physical, chemical, and biological systems, according to the universal principle of linearization of the relationship between input and output power coordinates at specific operating points. At the same time, the system is considered an energy converter (EC) with a certain number of inputs and outputs, but most often with one input and one output. For the latter case, a universal method of describing the EC using a system of dimensionless parameters and characteristics of its performance has been developed [2,18]. The most important indicator of an EC is the degree of coupling between its input and output, which shows what part of the input power is transferred to the EC output. Another part of the input power "slips through", which means that it is spent on organization of the process, but is not directly transferred to the output. The degree of coupling uniquely determines the maximum values of EC performance indicators, as well as the operating points at which these maximum values are reached. This makes it possible to optimize EC operation modes depending on the assumed optimization criteria [18]. This universal method was most widely used in bioenergetics to describe free energy transformations in biosystems, but it can be successfully used to analyze established processes of energy transformations in systems of any nature. For example, in [19], it was successfully applied to the analysis of energy conversion in electromechanics.

This work should be considered the first in the direction of the development of an applied method of the linear thermodynamics of non-equilibrium processes for further successful applications to complex objects of energy systems, in particular renewable energy systems. The universal approach to the mathematical description of systems of different natures, which is characteristic for this method, makes it possible to evaluate, from a common point of view, as universal ECs, each of the subsystems of a complex system with their parameters and maximum efficiency possibilities. As will be shown later in the work, significant reserves for improving the efficiency of the entire system lie in improving the conditions of the cascade connection of individual ECs, which most often takes place in different energy systems. In the work, a universal method of EC description was developed in the direction of the regularities of the cascade connection of two ECs, which makes it possible to evaluate the quality indicator of a specific connection and its influence on the efficiency indicators of the obtained equivalent cascade EC. For the successful application of the proposed method, a flow chart of the proposed approach of the investigation is given in Section 2.4. As a first test of this approach, the method of linear thermodynamics of non-equilibrium processes is applied to analyze the efficiency of energy conversion in the main WECS subsystems and to identify hidden opportunities for improving the efficiency of the entire system. In this work, the systems of linear equations were obtained for the first time for the steady-state modes of operation of two main ECs, which are the part of the WECS—a WT with a vertical axis of rotation (VAWT) and a vector controlled synchronous generator with permanent magnets (PMSG). Based on the obtained linear equations, these two ECs were described using a universal method. Taking into account the non-linear nature of steady-state processes in the VAWT and PMSG, systems of linear equations are obtained by linearizing the characteristics of these devices at operating points, and the mathematical model provides multiple linearization around the points of the optimal VAWT angular velocity at different wind speeds. In this paper, a universal method of EC description was also developed in the direction of the regularities of the cascade connection of two ECs, which makes it possible to evaluate the quality indicator of a specific connection and its influence on the efficiency indicators of the obtained equivalent cascade EC. Numerous studies conducted on the example of the studied WECS with specific VAWTs and PMSGs

showed the imperfection of the cascade connection of the latter, which increases with decreasing wind speed. The influence of parameters and characteristics of VAWT and PMSG on the quality of this connection was studied, and ways to improve it were outlined.

The paper is structured as follows: in Section 2, the main provisions of linear non-equilibrium thermodynamics and the universal method of describing and evaluating the performance indicators of linear ECs are briefly highlighted; in addition, this description is developed in relation to the cascade connection of two ECs and the method of energy optimization of the entire system steady-state operation mode is outlined; a mathematical description of the aeromechanical regularities of the WT as a linear EC and an evaluation of the effectiveness of the studied VAWT is carried out in Section 3; in Section 4, a mathematical description of the regularities of the operation of the vector-controlled PMSG as a linear EC was carried out, and the efficiency of the generator for the studied WECS was evaluated; in Section 5, an analysis of the efficiency of energy conversion in the "VAWT—PMSG" complex was carried out, and the influence of its parameters and characteristics on improving the quality of the connection between the studied VAWT and PMSG was investigated; concluding remarks are given in Section 6.

2. Indicators of EC Performance According to Linear Non-Equilibrium Thermodynamics

2.1. Basic Provisions of Linear Non-Equilibrium Thermodynamics

For any open system that exchanges energy and matter with the external environment, the entropy change is expressed by two components: $d_e S$—external, due to the exchange with the external environment (entropy flow); $d_i S$—internal, caused by non-equilibrium processes within the system (production of entropy). Based on this, the generalized form of the second law of thermodynamics for non-isolated systems is expressed based on the following dependency rate of entropy production in the system [3]:

$$\sigma_s = \frac{d_i S}{dt} \geq 0. \tag{1}$$

Since every real irreversible process is accompanied by some internal flow $\vec{J}_k$, generated by the corresponding driving force $\vec{X}_k$, which expresses disequilibrium, it has been proven [3] that in the conditions of local thermodynamic equilibrium (LTE), the following equality takes place:

$$\vec{J}_k = \sum_i L_{ki} \vec{X}_i. \tag{2}$$

The principle of LTE or microscopic reversibility, which is the basis of linear non-equilibrium thermodynamics, is that in the non-equilibrium state of the body during processes that are not very rapid, the state of its very small elements can be considered equilibrium, and the equations of classical thermodynamics can be applied to it [2]. The product of σ_s based on the absolute temperature of the system is called the dissipative function, because it reflects the rate of dissipation (scattering, degradation) of the free energy of the system.

A phenomenological law is also valid for LTE conditions, which expresses the intensity of any flow in the form of products of thermodynamic forces $\vec{X}_i$ and the corresponding kinetic coefficients L_{ki} (Onsager principle of linearity) [2,3]:

$$\sigma_s = \sum_i \vec{J}_k \vec{X}_k. \tag{3}$$

Expression (3) shows that one flow can be caused by different thermodynamic driving forces. However, according to the Curie principle [2], different driving forces can simultaneously affect the transfer if they are tensors of the same rank, for example, only scalars

or only vectors. In Expressions (2) and (3), flows and forces have a vector characteristic, which often happens in practice.

According to the second law of thermodynamics (1), the sum in Equation (2) must be greater than zero. However, this does not mean that each of the members of this sum must be individually greater than zero. Cases are possible when some members are positive, that is, they produce entropy, while others are negative, that is, and they consume an excess amount of entropy. This phenomenon, which consists of the fact that some processes can induce other processes to flow in a thermodynamically unfavorable direction (against the driving force, "downhill"), was called thermodynamic coupling [18]. Thus, for two coupling processes to which any EC belongs, since its output parameters (o—output) are determined by the input (i—input), the following system of equations can be written:

$$\begin{cases} J_i = L_{ii}X_i + L_{io}X_o \\ J_o = L_{oi}X_i + L_{oo}X_o \end{cases}, \quad (4)$$

where the kinetic or "phenomenological" coefficients are from the expressions

$$L_{jk} = \left(\frac{\partial J_j}{\partial X_k}\right)_{X_j=\text{const}}. \quad (5)$$

By definition, X_i, X_o, and J_i are positive, and J_o is negative, which means the absorption of energy at the input and its formation at the output; therefore, L_{ii}, L_{oo} and $-L_{io}$ must be positive.

L. Onsager discovered a general principle called Onsager reciprocal relations that can be called the fourth law of thermodynamics [18]. He claims that $L_{jk} = L_{kj}$, meaning that in the vicinity of the equilibrium state, the linear dependence of any flow J_j on any force X_k coincides with a similar dependence of flow J_k on force X_j. Onsager reciprocity ratios make it possible to significantly reduce the number of independent coefficients in systems of type (4). The validity of Onsager reciprocal relations is not limited to quasi-equilibrium systems (the reciprocity relations relate to the first derivatives of (5) at the equilibrium point), but their strength is higher the closer the system is to equilibrium. For significantly non-equilibrium systems, linear dependences (4) and reciprocity relations are often verified due to the validity of the LTE principle for individual small parts into which each large system is divided, which is under the influence of gradients of thermodynamic forces [18]. According to the second law of thermodynamics (1), limitations are imposed on the permissible values of kinetic coefficients—the matrix of coefficients L must be integrally defined, i.e.,

$$(L_{io})^2 \leq L_{ii}L_{oo}. \quad (6)$$

If mass and energy are transferred inside an isolated system under the influence of some forces, then the magnitude of this force decreases, and the system approaches a state of equilibrium, at which its entropy has a maximum value. The entropy of the system in any of its states is a measure of the system's approach to equilibrium, and the rate of its change over time (1), or the flow of entropy J_S, gives a quantitative assessment of the results of the transfer, which takes place under the influence of some driving forces. The smaller these forces are, the smaller the imbalance and the smaller the energy dissipation (2) and energy losses. For non-isolated systems, according to I. Prigozhin's minimum principle, the flow of entropy will acquire its smallest value in stationary processes, and it is clear that it will be smaller the slower the speed of this process [20].

2.2. A Universal Method of Describing and Evaluating Performance Indicators of Linear ECs

The above-described provisions of linear non-equilibrium thermodynamics are the basis of the theory of the thermodynamic analysis of ECs [2,18].

From the analysis of system (4), it is clear that the more negative the value of L_{io} (compared to the values of the remaining L coefficients), the higher the degree of influence

of the input force on the output flow. In addition, with more negative values L_{io}, the degree of suppression of the input flow by the force at the output increases. Thus, the coefficient L_{io} is related to the degree of coupling q between the input and output processes in EC. To avoid the effect on q values of other kinetic coefficients, the degree of coupling was defined as the coefficient L_{io} normalized to the coefficients L_{ii} and L_{oo} [18]:

$$q = \frac{L_{io}}{\sqrt{L_{ii}L_{oo}}}. \tag{7}$$

According to this definition, q will be negative and will acquire, taking into account (6), values from -1 to 0.

To obtain universal EC characteristics in relative units, two more indicators are introduced [18]:

- relation of forces

$$\chi = X_o / X_i; \tag{8}$$

- phenomenological relationship

$$Z = \sqrt{L_{oo}/L_{ii}}. \tag{9}$$

Having normalized the input and output fluxes to the input flux at zero output force (short circuit), the system of Equation (4) can be rewritten using the introduced notations:

$$\begin{cases} \frac{J_i}{L_{ii}X_i} = q \cdot (Z\chi) + 1 \\ \frac{J_o}{ZL_{ii}X_i} = (Z\chi) + q \end{cases} \tag{10}$$

and the flow ratio ca be determined as follows:

$$j = \frac{J_o}{J_i} = Z\frac{(Z\chi) + q}{q \cdot (Z\chi) + 1}. \tag{11}$$

In expressions (10) and (11), the product $(Z\chi)$ is a dimensionless number that expresses the reduced force ratio. The content of q also becomes clear: when $q = -1$ the output flow differs from the input flow always by Z times; therefore, the flows are rigidly (completely) coupled. When $q = 0$ the input and output flows are caused only by their own forces and flow in the direction of their decrease, which means that the flows are not coupled at all. For values of q from –1 to 0 the output flow is supported by the input flow in the "downhill" direction, but the ratio of these flows changes along with the change in $(Z\chi)$, which means that the input and output processes in this case are partially coupled.

An important characteristic of ECs is the thermodynamic efficiency of their operation, i.e., the ratio of the rate at which the EC produces free output energy to the rate at which it consumes free input energy:

$$\eta = -\frac{J_o X_o}{J_i X_i} = -j\chi = -(Z\chi)\frac{(Z\chi) + q}{q \cdot (Z\chi) + 1}. \tag{12}$$

Graphical dependence (12) at different values of q is shown in Figure 1a. From (12), it is easy to find the optimal ratio of forces from the point of view of thermodynamic efficiency:

$$(Z\chi)_{opt-\eta} = -\frac{q}{1 + \sqrt{1 - q^2}}, \tag{13}$$

at which the thermodynamic efficiency has a maximum value equal to

$$\eta_{max} = (Z\chi)^2_{opt-\eta}. \tag{14}$$

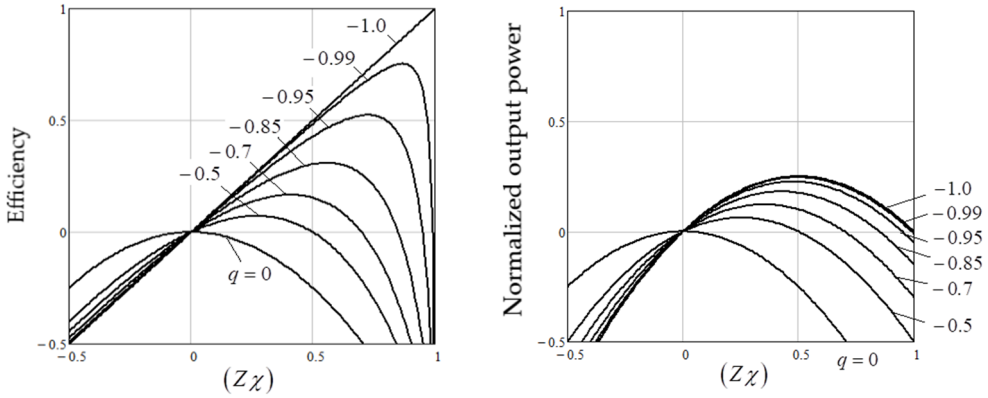

(**a**) (**b**)

Figure 1. Dependencies of efficiency (**a**) and normalized output power (**b**) on the reduced force ratio at different degrees of coupling q.

The operation of EC at the point with maximum thermodynamic efficiency is attractive at first glance, but at high degrees of coupling ($|q| \to 1$), it may be impractical, since the output flow approaches zero, meaning the output process proceeds at a very low speed. To achieve energy conversion at a higher speed, it is necessary to partially sacrifice thermodynamic efficiency.

One of the expedient options for choosing the EC operating point can be the maximum output power mode. The normalized value of the output power can be expressed as follows:

$$p = -\frac{J_o X_o}{L_{ii} X_i^2} = -[(Z\chi) + q] \cdot (Z\chi). \tag{15}$$

Graphic dependence (15) at different q value is shown in Figure 1b. The maximum output power is reached at

$$(Z\chi)_{P.max} = -q/2 \tag{16}$$

and is

$$p_{max} = q^2/4. \tag{17}$$

However, as can be seen from Figure 1a,b, the maximum output power is accompanied by a rather low thermodynamic efficiency and can be recommended only for ECs connected to free energy sources, for example, natural renewable ones.

Using the obtained universal dependencies (10)–(12) and (15), combining two indicators, it is possible to easily form other optimal operation criteria appropriate for specific ECs [18], for example maximum output flow at optimal thermodynamic efficiency, maximum output power at optimal thermodynamic efficiency, maximum product $[J_o/(ZL_{ii}X_i)] \cdot \eta$ (so-called "economically profitable output flow"), maximum product $p\eta$ (so-called "economically profitable output power"), etc. The technique of ensuring the indicated optimal mode consists of changing the available kinetic coefficients of the original model (4) in such a way to obtain the required combination of parameters $(Z\chi)$ and q, at which the selected criterion reaches its maximum value.

2.3. Performance Indicators of Cascaded Linear ECs

The analysis shows that elementary ECs in energy conversion systems are most often connected in cascade. For a mathematical description of the steady-state mode of operation at a given point of a system of two cascaded ECs (marked by indices 1 and 2), we will use the following systems of linear equations:

$$\begin{cases} J_1^i = L_1^{ii} X^i + L_1^{io} X^o \\ J_1^o = L_1^{oi} X^i + L_1^{oo} X^o \end{cases} ; \begin{cases} J_2^i = L_2^{ii} X^i + L_2^{io} X^o \\ J_2^o = L_2^{oi} X^i + L_2^{oo} X^o \end{cases} . \tag{18}$$

For the cascade connection of such ECs, the following conditions apply: $X_1^{\text{o}} = X_2^{\text{i}}$, $J_1^{\text{o}} = J_2^{\text{i}}$. If such a cascade is considered a new equivalent EC, then after mathematical transformations, its parameters are found, which are determined based on the parameters of the ECs, from which it is composed:

$$q_\Sigma = \frac{q_1 q_2}{\sqrt{\left(1 - q_1^2 + \gamma\right)\left(1 - q_2^2 + \gamma^{-1}\right)}};\ Z_\Sigma = Z_1 Z_2 \gamma \sqrt{\frac{1 - q_2^2 + \gamma^{-1}}{1 - q_1^2 + \gamma}};\ \chi_\Sigma = \chi_1 \chi_2, \tag{19}$$

where γ is the connection coefficient of two ECs in the cascade, which is equal to

$$\gamma = \frac{L_2^{\text{ii}}}{L_1^{\text{oo}}}. \tag{20}$$

Figure 2 shows the graphical dependence $q(\gamma)$ at the given $q_1 = -0.95$ and $q_2 = 0.86...0.98$ (for a better understanding, the abscissa axis is presented using a logarithmic scale). As can be seen, for any q_1 and q_2, there exists some optimal connection coefficient at which the total degree of conjugation is maximal. This optimal value of the connection coefficient is obtained in the form

$$\gamma_{\text{opt}} = \sqrt{\frac{1 - q_1^2}{1 - q_2^2}}. \tag{21}$$

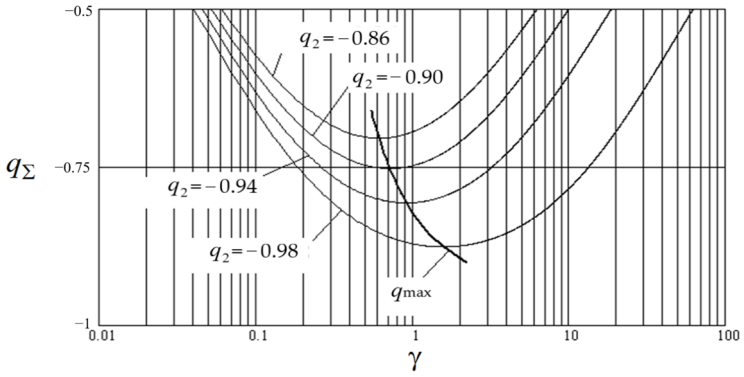

Figure 2. Dependencies of the degree of coupling for an equivalent EC on the connection coefficient of two ECs at given values of the degrees of coupling of EC 1 ($q_1 = -0.95$) and EC 2 ($q_2 = 0.86...0.98$).

With an optimal connection, the maximum conjugation of two ECs is characterized by the following degree of coupling:

$$q_{\Sigma.\max} = \frac{q_1 q_2}{\sqrt{\left(1 - q_1^2\right)\left(1 - q_2^2\right)} + 1} \tag{22}$$

and the optimal reduced force ratio is equal to

$$(Z\chi)_{\Sigma.\text{opt}} = (Z\chi)_1 (Z\chi)_2. \tag{23}$$

2.4. The Energy Optimization Method of the Stady-State Operation Mode of the System

Based on the above, it is possible to propose a method of energy optimization of the steady-state operation of the system under study, which consists of the five steps, as is shown in Figure 3.

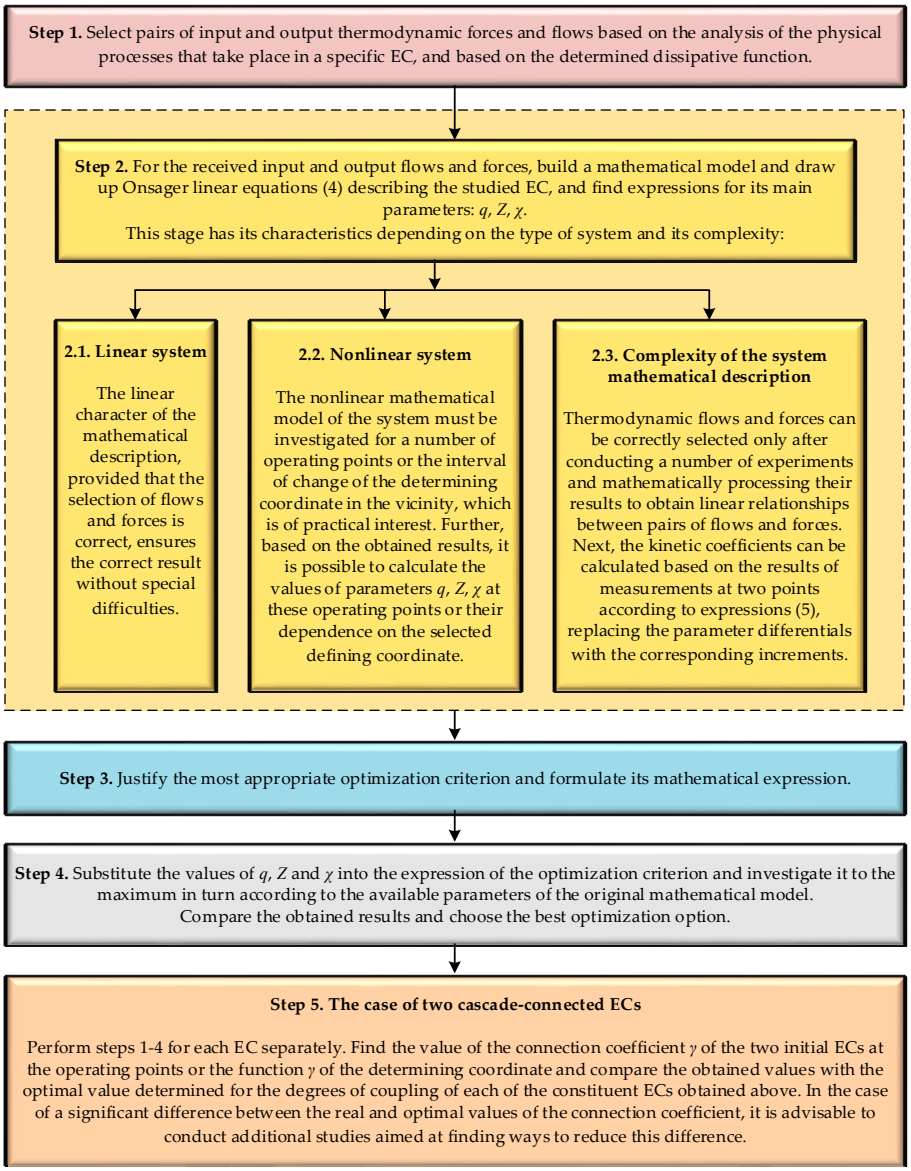

Figure 3. Flow chart of the application of the proposed approach.

3. Thermodynamic Analysis of Energy Conversion Efficiency in WT

3.1. Mathematical Description of the Aeromechanical Regularities of WT Operation as a Linear EC

The mechanical power on the axis of WT depends on wind velocity V_w and is determined using the following equation [21]:

$$P_{WT} = 0.5\rho S C_P(\lambda) {V_w}^3, \tag{24}$$

where ρ is the air density, S is the swept area of WT, $C_P(\lambda)$ is the wind power conversion efficiency factor of WT, λ is the tip speed ratio (TSR), ω is the turbine angular velocity, and R is the radius of WT.

TSR is the linear speed of the blade edge relative to the wind speed:

$$\lambda = \frac{\omega R}{V_w}. \tag{25}$$

The dimensionless aeromechanical characteristic $C_P(\lambda)$ uniquely determines the appearance of the characteristics $P_{WT}(\omega, V_w)$, which are scaled along the P_{WT} and ω axes depending on the power (dimensions) of the WT. The $C_P(\lambda)$ characteristic, which is ob-

tained through complex experimental or model studies, is often represented based on a polynomial dependence of the n-th degree:

$$C_P(\lambda) = \sum_{i=0}^{n} a_i \lambda^i. \quad (26)$$

To provide maximum power extraction from the wind, according to Equation (24), it is necessary to maintain the maximum value of the power factor $C_{Pmax}(\lambda_{opt})$ and therefore an optimal WT angular velocity,

$$\omega_{opt} = \frac{\lambda_{opt}}{R} V_w, \quad (27)$$

which is achieved by the automatic regulation of the load torque at a WT shaft.

In the steady state, the torque of a WT is balanced by the load torque, which, based on (24) and (25), is described by the following expression:

$$T_{WT} = \frac{P_{WT}}{\omega} = 0.5\rho SR \frac{C_P(\lambda)}{\lambda} {V_w}^2. \quad (28)$$

As an EC, the WT converts the power of the wind flow into the power of rotational motion on the WT shaft. At the input of this EC, there is a force in the form of the speed of the wind flow $X_i = V_w$, which determines the input flow in the form of a force acting on the WT $J_i = F$. At the output of the EC, the force in the form of angular velocity determines the torque on the WT shaft: $X_o = \omega$, $J_o = T_{WT}$. Powers at the input and output of EC are respectively equal to $P_i = V_w F$ and $P_o = \omega T_{WT}$.

Similarly to (4), the system of linear equations that describes the operation of the WT as an EC will have the form

$$\begin{cases} F = L_{ii} V_w + L_{io} \omega \\ -T_{WT} = L_{oi} V_w + L_{oo} \omega \end{cases}. \quad (29)$$

As can be seen from the mathematical description (24)–(28), the mathematical model of the processes in WT is significantly nonlinear; therefore, the system of linear Equation (29) is valid only in the vicinity of some given operating point. Figure 3 shows a typical dependence $T_{WT}(\omega)$ with the point of optimal operation $T_{WT.opt}(\omega_{opt})$, in which the maximum WT power value (maximum power point—MPP) $P_{WT.max}$ is provided. Shown in Figure 4, tangent 1 to this point is described based on the second equation of the system (29), if this system is intended to simulate the operation of the WT in the MPP. Let us determine the expressions for the kinetic coefficients in the system of equations (29) using the example of the WT operation at this point.

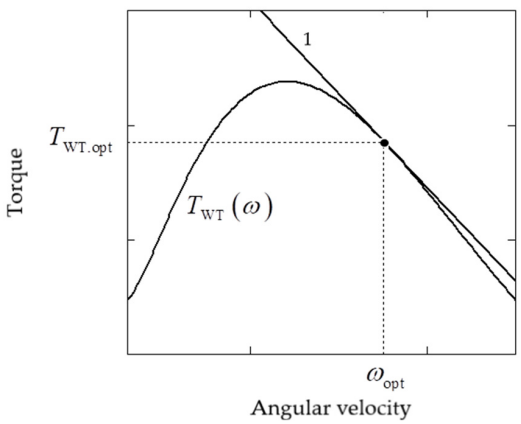

Figure 4. View of the $T_{WT}(\omega)$ characteristic with its linearization at the point of optimal WT operation.

The equation of the tangent curve shown in the Figure 4 has the form

$$T_{\mathrm{WT}} = k\omega + b, \tag{30}$$

where

$$k = \left.\frac{\mathrm{d}T_{\mathrm{WT}}}{\mathrm{d}\omega}\right|_{\omega=\omega_{\mathrm{opt}}} = 0.5\rho S R {V_{\mathrm{w}}}^2 \left.\frac{\mathrm{d}}{\mathrm{d}\omega}\left(\frac{C_{\mathrm{P}}(\lambda)}{\lambda}\right)\right|_{\omega=\omega_{\mathrm{opt}}} = 0.5\rho S R {V_{\mathrm{w}}}^2 \left.\left[\frac{\mathrm{d}}{\mathrm{d}\lambda}\left(\frac{C_{\mathrm{P}}(\lambda)}{\lambda}\right)\cdot\frac{\mathrm{d}\lambda}{\mathrm{d}\omega}\right]\right|_{\omega=\omega_{\mathrm{opt}}}, \tag{31}$$

$$b = T_{\mathrm{WT.opt}} + k\omega_{\mathrm{opt}}. \tag{32}$$

Considering (25) and introducing the notation $B = 0.5\rho S R^2 V_{\mathrm{w}}$, the Equation (31) will have the form

$$k = B\left.\frac{\mathrm{d}}{\mathrm{d}\lambda}\left(\frac{C_{\mathrm{P}}(\lambda)}{\lambda}\right)\right|_{\lambda=\lambda_{\mathrm{opt}}}. \tag{33}$$

For ω = 0, from the second equation of system (29), we obtain

$$L_{\mathrm{oi}} = -\frac{T_{\mathrm{WT}}|_{\omega=0}}{V_{\mathrm{w}}} = -\frac{b}{V_{\mathrm{w}}}. \tag{34}$$

For $T_{\mathrm{WT}} = 0$, $\omega = -b/k$ follows from Equation (30). Then, from the second equation of system (29), we obtain

$$L_{\mathrm{oo}} = -L_{\mathrm{oi}}\frac{V_{\mathrm{w}}}{\omega} = \frac{b}{\omega} = -k. \tag{35}$$

For the estimated optimal operating point from the first equation of the system (29) we obtain

$$L_{\mathrm{ii}} = \frac{F - L_{\mathrm{io}}\omega_{\mathrm{opt}}}{V_{\mathrm{w}}}, \tag{36}$$

where $F = 0.5\rho S {V_{\mathrm{w}}}^2$ is the value of the force of the wind flow pressure on the WT depending on the wind speed V_{w}.

3.2. The Main Performance Indicators of the Experimental WT

The aeromechanical characteristic of a VAWT taken for the study is shown in Figure 5 and is described based on the following polynomial

$$C_{\mathrm{P}}(\lambda) = \sum_{i=0}^{n} a_i \lambda^i = 0.046977 - 0.128468\lambda + 0.19596\lambda^2 - 0.05705\lambda^3 + 0.00621\lambda^4 - 0.000236\lambda^5. \tag{37}$$

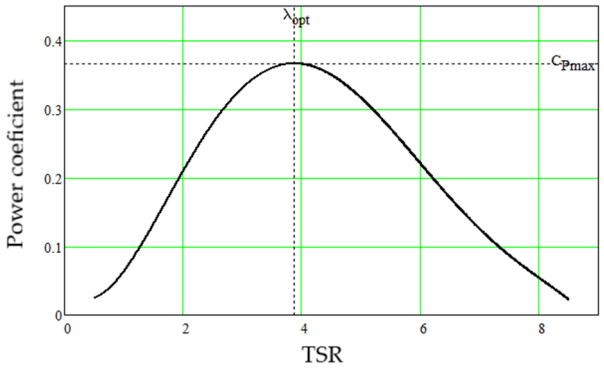

Figure 5. Power coefficient vs. TSR for the studied VAWT.

The main parameters of the experimental VAWT are given in Table 1.

Table 1. Parameters of the VAWT.

Parameters	Value
Rated power, $P_{WT\cdot n}$ (kW)	10
Rated wind speed, V_w (m/s)	12
Maximum of power coefficient, $C_{p\cdot max}$	0.3661
Optimum value of TSR, λ_{opt}	3.873
Rotor radius, R (m)	2.65
Rotor high, H (m)	1.25
Air density, ρ (kg/m^3)	4.78

Figure 6 shows the dependences of the torque of the experimental VAWT on its angular velocity for three values of wind speed—8 m/s, 10 m/s, and 12 m/s. Similarly to the one shown in Figure 4, the linearized dependences $T_{WT}(\omega)$ are shown by lines 1, 2, and 3, respectively, at the optimal points of the maximum VAWT power $T_{WT.opt}(\omega_{opt})$.

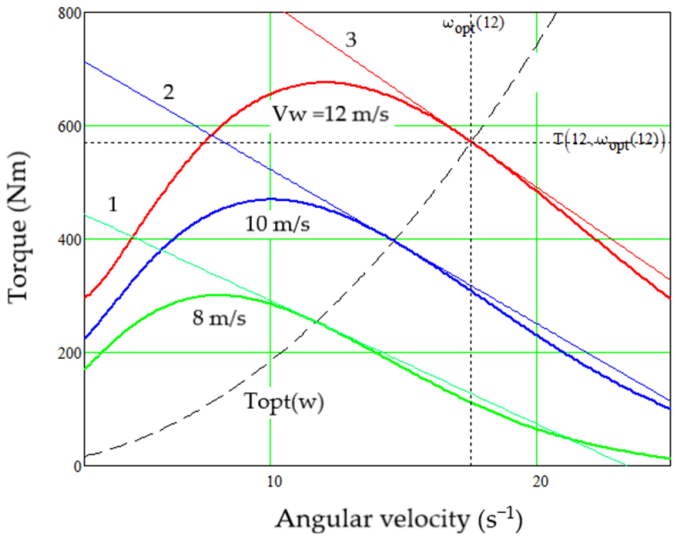

Figure 6. VAWT torque vs. its angular velocity at different wind speeds.

As can be seen from Figure 6, near the selected points, the obtained straight lines have small deviations from the linearized curves, and the parameters k and b of these straight lines are different. This is confirmed based on the results of calculations based on Expressions (33) and (32). However, regardless of this, calculations according to Expressions (34)–(36) lead to the same results regarding the main parameters of the VAWT as a linear EC for linearized characteristics at the points of optimal operation of the experimental WT at different wind speeds: degree of coupling $q = -0.9192$, reduced force ratio $(Z\chi) = 0,4602$. The dependences of the thermodynamic efficiency and the normalized value of the output power, obtained from Expressions (12) and (15), respectively, for these parameters are shown in Figure 7. As can be seen from the figure, the value $(Z\chi) = 0.4602$ is optimal for the normalized value of the output power, at which its maximum value $p_{max} = 0.2112$ is reached according to (17). This corresponds to the optimal operation mode of the VAWT, designed to obtain the maximum power value from the wind at any wind speed (in the range of incomplete VAWT power—from the starting to the nominal wind speed). At the same time, given the obtained value $(Z\chi) = 0.4602$, the thermodynamic efficiency of converting wind power into mechanical power of the WT rotor is not maximal.

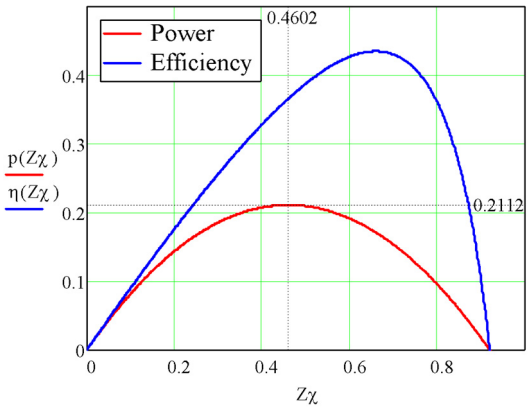

Figure 7. Dependencies of $p(Z\chi)$ and $\eta(Z\chi)$, obtained for the experimental VAWT as an EC linearized at the point of optimal operation of the VAWT.

Figure 8 shows the dependences of the absolute power values of the studied VAWT on its angular velocity (curves 1), obtained based on (15), for three values of the wind speed according to the following expression:

$$P_{\mathrm{WT.opt}}(\omega) = L_{\mathrm{ii}}\left(V_{\mathrm{w}}, \omega_{\mathrm{opt}}\right) F(V_{\mathrm{w}})^2 \left[\left(Z_{\mathrm{opt}}\chi(\omega)\right) + q_{\mathrm{opt}}\right] \cdot \left(Z_{\mathrm{opt}}\chi(\omega)\right), \tag{38}$$

where the index opt indicates the corresponding parameters determined for the points of optimal operation of the experimental VAWT, at which the maximum value of the output power is ensured at a specific wind speed.

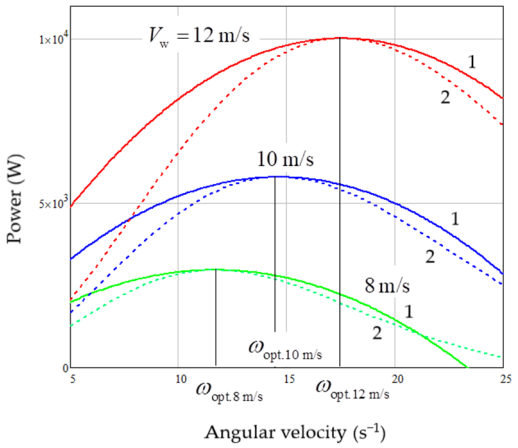

Figure 8. Dependences of the output power of the studied VAWT on its angular velocity at different wind speeds.

As expected, at optimal angular velocity values, the output power of the studied VAWT reaches its maximum value. However, as can be seen from Figure 4, when the angular velocity deviates from the optimum, the real WT torque decreases compared to the linearized values corresponding to straight line 1. This means, for deviations from the point of optimal operation, the accuracy of VAWT modeling based on the linear EC decreases. In the future, after consideration of the entire WECS, optimization of its operation will be ensured based on the system criterion—the maximum electrical power received at the output of the generator. This will mostly lead to some deviation of the operating point of the VAWT from its optimal mode. Therefore, in order to increase the accuracy of the mathematical description, it is advisable to model the VAWT, not based on one linear EC, as was performed above, but based on a whole series of ECs with slightly different parameters obtained for the current VAWT angular velocity by linearizing the characteristic $T_{\mathrm{WT}}(\omega)$ at this point. For this purpose, a special program has been developed

in the MathCad environment, which determines the dependence of all parameters and variables on the angular velocity of the VAWT in the given vicinity of its MPP, i.e., performs multiple linearization of the characteristics $T_{WT}(\omega)$ for the given wind speeds of 8 m/s, 10 m/s, and 12 m/s. As a result of such modeling, the kinetic coefficients of the system of Equation (29), determined for each wind speed, will also depend on the VAWT angular velocity. Consequently, this will also lead to the dependence of the main VAWT parameters, such as EC, on the angular velocity—degree of coupling q_{WT} and normalized force ratio $(Z\chi)_{WT}$. As a result of the conducted research, the following dependencies of the specified parameters for the studied VAWT at the three specified wind speeds are presented in Figure 9. As can be seen from the given dependencies, the trends of their change are in contradiction: with an increase in angular velocity, q_{WT} decreases by a modulus, but $(Z\chi)_{WT}$ increases and, conversely, with a decrease in angular velocity, q_{WT} increases by a modulus, but $(Z\chi)_{WT}$ decreases. In both cases, this will lead to a deviation from the points of optimal operation marked in the figures. As proof, numbers 2 in Figure 8 indicate the dependences of the output power of the studied VAWT on its angular velocity at different wind speeds, which are similar to those indicated by numbers 1 and obtained only for the MPP operation of the studied VAWT. As can be seen, curve 2 is characterized by a sharper decrease in VAWT output power than curve 1 for deviations from the MPP.

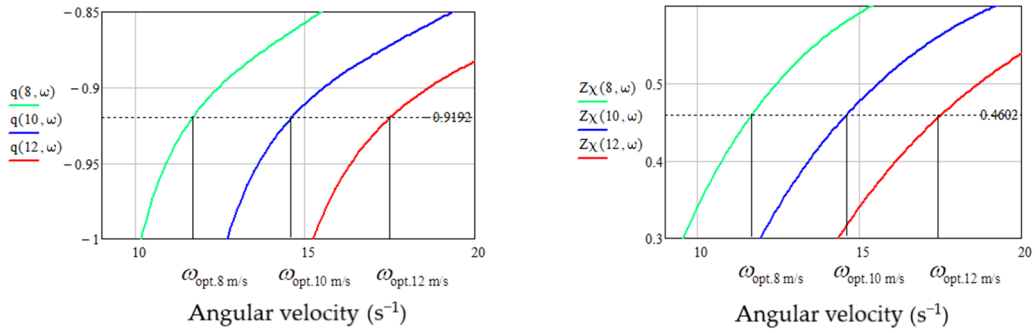

Figure 9. Dependencies of the main parameters of ECs that simulate the operation of the studied VAWT at different wind speeds on the angular velocity of the VAWT: (**a**) the degree of coupling q, (**b**) the reduced force ratio $(Z\chi)$.

4. Thermodynamic Analysis of the PMSG Energy Conversion Efficiency

4.1. Mathematical Description of Mechano-Electrical Regularities of PMSG Operation as a Linear EC

Taking into account losses in both copper and steel, the mathematical model of the PMSG operation in a *d-q* orthogonal reference frame, rotating with the rotor and oriented along the rotor field, can be obtained from the corresponding two-phase substitute circuit, which is shown in Figure 10 [22]. The diagram shows (the indices d and q refer to the corresponding axes of the coordinate system) the following: u_d, u_q are the projections of the armature voltage vector at the generator output; i_d, i_q are the projections of the armature current vector at the generator output; i_{d0}, i_{q0} are the projections of the armature current vector, which forms the electromagnetic torque of the generator; R_a is the active resistance of the armature winding; L_d, L_q are the armature winding inductances relative to the axes d and q; R_c is the active resistance simulating losses in generator steel; i_{dc}, i_{qc} are the projections of the armature current vector, which simulates losses in the generator steel; ω is the angular speed of the generator rotor; p is the number of generator pole pairs; ψ_{pm} is the flux-coupling amplitude created by one pair of permanent magnet poles.

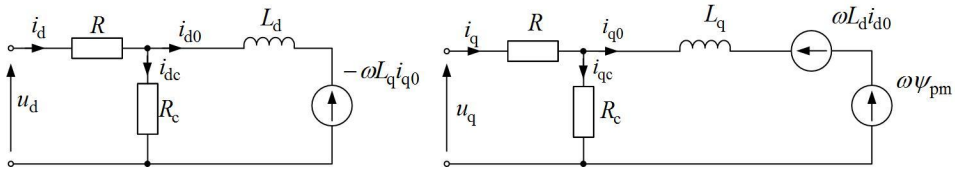

Figure 10. PMSG replacement scheme taking into account losses in steel.

Based on the schemes presented in Figure 10, the equation of the electrical balance of currents and voltages in the *d-q* projections under the steady-state mode of operation of the PMSG can be described using the following systems of equations [23]:

$$\begin{cases} i_q = i_{q0} + i_{d0}\frac{p\omega L_d}{R_c} - \frac{p\omega\psi_{pm}}{R_c} \\ i_d = i_{d0} - i_{q0}\frac{p\omega L_q}{R_c} \end{cases}; \tag{39}$$

$$\begin{cases} u_q = -i_q R_a - p\omega L_d i_{d0}\left(1 + \frac{R_a}{R_c}\right) + p\omega\psi_{pm}\left(1 + \frac{R_a}{R_c}\right) \\ u_d = -i_d R_a + p\omega L_q i_{q0}\left(1 + \frac{R_a}{R_c}\right) \end{cases}. \tag{40}$$

We will assume that the permanent magnets are placed on the surface of the rotor (surface-mounted PMSM—SPMSM), for which $L_d = L_q = L_a$, which mostly occurs in the real WECS [24]. Then, the electromagnetic torque created by the generator is as follows:

$$T_G = \frac{3}{2} p\psi_{pm} i_{q0}. \tag{41}$$

Control of the PMSG load torque is carried out, most often, in a vector way using an active rectifier that is implemented by forming the armature current in phase with the EMF of the generator, i.e., ensuring the condition $i_d = 0$ [25].

As an EC, the PMSG converts the mechanical power of the WT on its shaft into electrical power at the output of the generator armature winding. At the input of this EC, there is a force in the form of the rotor angular velocity $X_i = \omega$, which determines the input flow in the form of the rotation WT torque, which in the steady-state, is equal to the braking PMSG electromagnetic torque $J_i = T_G$. At the EC output, the force in the form of the armature voltage vector determines the armature current vector: $X_o = \vec{u}_a$, $J_o = \vec{i}_a$. The power at the EC input is $P_i = \omega T_G$, and the power at its output is the dot product of the armature voltage and current vectors. $P_o = \left(\vec{u}_a \cdot \vec{i}_a\right)$. The last expression, taking into account the vector control strategy $i_d = 0$, will take the following form:

$$P_o = \left(\vec{u}_a \cdot \vec{i}_a\right) = \frac{3}{2}\left(u_d i_d + u_q i_q\right) = \left(\sqrt{\frac{3}{2}} u_q\right)\left(\sqrt{\frac{3}{2}} i_q\right), \tag{42}$$

where the factor 3/2 is due to the transformation of the three-phase reference frame to the two-phase one.

Based on (42), the output force and flow of the EC will be as follows: $X_o = \sqrt{\frac{3}{2}} u_q$, $J_o = \sqrt{\frac{3}{2}} i_q$.

Similarly to (4), the system of linear equations that describes the operation of the PMSG as an EC will have the form

$$\begin{cases} T_G = L_{ii}\omega + L_{io}\left(\sqrt{\frac{3}{2}} u_q\right) \\ -\left(\sqrt{\frac{3}{2}} i_q\right) = L_{oi}\omega + L_{oo}\left(\sqrt{\frac{3}{2}} u_q\right) \end{cases}. \tag{43}$$

Let us determine the kinetic coefficients in the system of Equation (43) using the PMSG mathematical model (39)–(41).

Given that $i_{\mathrm{d}} = 0$, from the second equation of system (39), we obtain

$$i_{\mathrm{d0}} = i_{\mathrm{q0}} \frac{p\omega L_{\mathrm{a}}}{R_{\mathrm{c}}}. \tag{44}$$

The analysis of Expression (44) shows that i_{d0} has a much smaller value compared to i_{q0} due to the small factor near the latter. When substituting i_{d0} into the first equation of system (39), this small factor at i_{q0} will already be squared, so the second terms on the right side of this equation can be neglected without the risk of losing the accuracy of the mathematical description. Having performed this and substituting i_{q} from the first equation of system (39) into the first equation of system (40), after transformations, we obtain

$$i_{\mathrm{q0}} = -\frac{u_{\mathrm{q}}}{AR_{\mathrm{a}}} + \frac{p\omega\psi_{\mathrm{pm}}}{AR_{\mathrm{a}}}\left(1 + \frac{2R_{\mathrm{a}}}{R_{\mathrm{c}}}\right), \tag{45}$$

where

$$A = 1 + \frac{(p\omega L_{\mathrm{a}})^2}{R_{\mathrm{a}}R_{\mathrm{c}}}\left(1 + \frac{R_{\mathrm{a}}}{R_{\mathrm{c}}}\right). \tag{46}$$

Substituting (45) into (41), we obtain the first equation of system (43) in the form

$$T_{\mathrm{G}} = \frac{3}{2}\frac{(p\psi_{\mathrm{pm}})^2}{AR_{\mathrm{a}}}\left(1 + \frac{2R_{\mathrm{a}}}{R_{\mathrm{c}}}\right)\omega - \sqrt{\frac{3}{2}}\frac{p\psi_{\mathrm{pm}}}{AR_{\mathrm{a}}}\left(\sqrt{\frac{3}{2}}u_{\mathrm{q}}\right). \tag{47}$$

Substituting (45) into the first equation of system (39), we obtain

$$-i_{\mathrm{q}} = -\frac{p\psi_{\mathrm{pm}}}{AR_{\mathrm{a}}}\omega\left[1 + \frac{R_{\mathrm{a}}}{R_{\mathrm{c}}}(2 - A)\right] + \frac{1}{AR_{\mathrm{a}}}u_{\mathrm{q}}. \tag{48}$$

An analysis of the expression in square brackets shows that its value differs from unity by tenths of a percent, so it can be replaced by unity. Multiplying both parts of Equation (48) by $\sqrt{3/2}$, we obtain the second equation of system (43) in the form

$$-\left(\sqrt{\frac{3}{2}}i_{\mathrm{q}}\right) = -\sqrt{\frac{3}{2}}\frac{p\psi_{\mathrm{pm}}}{AR_{\mathrm{a}}}\omega + \frac{1}{AR_{\mathrm{a}}}\left(\sqrt{\frac{3}{2}}u_{\mathrm{q}}\right). \tag{49}$$

From the equations of the system composed of Equations (47) and (49), we obtain the expressions for the kinetic coefficients of the EC, which describe the operation of the vector-controlled PMSG:

$$L_{\mathrm{ii}} = \frac{3}{2}\frac{(p\psi_{\mathrm{pm}})^2}{AR_{\mathrm{a}}}\left(1 + \frac{2R_{\mathrm{a}}}{R_{\mathrm{c}}}\right),\ L_{\mathrm{io}} = -\sqrt{\frac{3}{2}}\frac{p\psi_{\mathrm{pm}}}{AR_{\mathrm{a}}},\ L_{\mathrm{oo}} = \frac{1}{AR_{\mathrm{a}}}. \tag{50}$$

Having the expressions for the kinetic coefficients (50), it is possible to obtain from (5)–(7) the expressions for the main dimensionless parameters of this EC:

$$q_{\mathrm{G}} = -\left(1 + \frac{2R_{\mathrm{a}}}{R_{\mathrm{c}}}\right)^{-0.5},\ Z_{\mathrm{G}} = (p\psi_{\mathrm{pm}})^{-1}\left[\frac{3}{2}\left(1 + \frac{2R_{\mathrm{a}}}{R_{\mathrm{c}}}\right)\right]^{-0.5},\ \chi_{\mathrm{G}} = \sqrt{\frac{3}{2}}\frac{u_{\mathrm{q}}}{\omega}. \tag{51}$$

Using Equations (45) and (51), we finally obtain

$$(Z\chi)_{\mathrm{G}} = \left(1 + \frac{2R_{\mathrm{a}}}{R_{\mathrm{c}}}\right)^{0.5}\left[1 - \frac{AR_{\mathrm{a}}i_{q0}}{p\omega\psi_{\mathrm{pm}}(1 + 2R_{\mathrm{a}}/R_{\mathrm{c}})}\right]. \tag{52}$$

4.2. Determination of the Parameters of the Studied PMSG

For further research, it is necessary to obtain the parameters of the studied PMSG, which will work together with the VAWT, the parameters of which are given in Table 1. Let us find, with a reasonable approximation, expressions for determining the main parameters of the generator, based on its given energy indicators—relative energy losses in copper δ_{Cu} and steel δ_{Fe}.

In the case of a PMSG with its specified nominal input parameters (torque T_{n} and angular velocity ω_{n}), its parameters, such as p and ψ_{pm}, determine the level of output parameters—nominal values of voltage and armature current, which in this study, are of no fundamental importance. Therefore p and ψ_{pm} can be chosen arbitrarily, within the limits of real values.

To determine the value of the resistance of the generator armature, we will neglect the losses in the steel and take $R_{\mathrm{c}} = \infty$. Then, the relative energy losses in copper in the case of a vector-controlled PMSG in the nominal mode will be as follows:

$$\delta_{\mathrm{Cu}} = \frac{\Delta P_{\mathrm{Cu}}}{P_{\mathrm{mech}} + \Delta P_{\mathrm{Cu}}} = \frac{3/2 \cdot i_{\mathrm{q0.n}}^2 R_{\mathrm{a}}}{3/2 \cdot p\psi_{\mathrm{pm}} i_{\mathrm{q0.n}} \omega_{\mathrm{n}} + 3/2 \cdot i_{\mathrm{q0.n}}^2 R_{\mathrm{a}}} = \left(\frac{p\omega_{\mathrm{n}}\psi_{\mathrm{pm}}}{i_{\mathrm{q0.n}} R_{\mathrm{a}}} + 1 \right)^{-1}, \quad (53)$$

where ΔP_{Cu} is the absolute power loss in copper, P_{mech} is the mechanical power of PMSG, and $i_{\mathrm{q0.n}}$ is the nominal value of the projection of the armature current onto the q axis.

From (53) we obtain

$$R_{\mathrm{a}} = \frac{p\omega_{\mathrm{n}}\psi_{\mathrm{pm}}}{i_{\mathrm{q0.n}} \left(\delta_{\mathrm{Cu}}^{-1} - 1 \right)}. \quad (54)$$

The inductance of the PMSG armature winding and other parameters affect the magnitude of the shift angle φ between the armature voltage $\vec{v}$ and current $\vec{i}$ vectors. From the vector diagram (Figure 11) for the nominal mode of a synchronous machine with magnets placed on the surface of the rotor, taking into account that its armature current $i = i_{\mathrm{q0.n}}$, and EMF $e = p\omega_{\mathrm{n}}\psi_{\mathrm{pm}}$, the following can be written:

$$\mathrm{tg}\varphi = \frac{p\omega_{\mathrm{n}} L_{\mathrm{a}} i_{\mathrm{q0.n}}}{p\omega_{\mathrm{n}}\psi_{\mathrm{pm}} + i_{\mathrm{q0.n}} R_{\mathrm{a}}}. \quad (55)$$

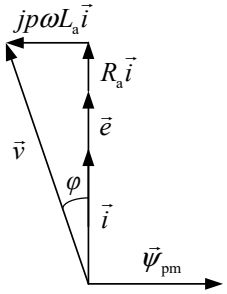

Figure 11. Vector diagram of a vector-controlled synchronous machine with permanent magnets placed on the surface of the rotor.

From (55), we receive

$$L_{\mathrm{a}} = \left(\frac{\psi_{\mathrm{pm}}}{i_{\mathrm{q0.n}}} + \frac{R_{\mathrm{a}}}{p\omega_{\mathrm{n}}} \right) \mathrm{tg}\varphi. \quad (56)$$

From the scheme shown in Figure 10, the relative power losses in PMSG steel can be represented by the power losses in the resistance R_{c}. For the nominal mode of PMSG operation, the following can be written:

$$\delta_{\mathrm{Fe}} = \frac{\left(p\omega_{\mathrm{n}}\psi_{\mathrm{pm}} \right)^2}{R_{\mathrm{c.n}} P_{\mathrm{n}}}, \quad (57)$$

where $R_{c.n}$ is the resistance R_c value at the nominal operation mode of the PMSG, and P_n is the rated power of the PMSG.

Since power losses due to hysteresis and eddy currents, which together make up losses in steel, depend in different ways on the angular velocity of the machine, the resistance R_c value decreases as the speed decreases. As shown in [26], such a trend can be modeled using the following equation:

$$R_c = R_{c.n} \frac{\frac{K_f}{K_h} + 1}{\frac{K_f}{K_h} + \frac{1}{\omega^*}}, \quad (58)$$

where K_h and K_f are the relative values of power losses due to hysteresis and eddy currents for the nominal PMSG mode (according to experimental data [23], we adopt $K_f/K_h = 0.5694$).

The PMSG parameters adopted and calculated using expressions (54), (56), and (57) are given in Table 2.

Table 2. Parameters of the studied PMSG.

Parameters	Value
Rated power, $P_{G\cdot n}$ (kW)	10
Rated angular velocity, $\omega_{G\cdot n}$ (s^{-1})	17.54
Rated torque, $T_{G\cdot n}$ (Nm)	570.2
Number of pole pairs, p	24
PM flux linkage, ψ_{pm} (Wb)	0.41
Relative losses in copper, δ_{Cu}	0.07
Relative losses in steel, δ_{Fe}	0.03
Angle of shift between armature voltage and current, φ (deg)	30
Winding resistance, R_a (Ω)	0.286
Winding inductance, L_a (mH)	6.1
Rated equivalent iron loss resistance, $R_{c\cdot n}$ (Ω)	84.4

4.3. Thermodynamic Performance Indicators of the Studied PMSG

To evaluate the parameters of the studied PMSG, the following computational experiment was conducted. The generator is set in motion by an external motor with such torque to ensure its given angular velocity regardless of the electrical load of the generator. Based on the obtained expressions (51) and (52), dependencies of the main parameters of the generator as the EC on the given angular velocity were calculated for three such values of the electric load of the generator, which form its electromagnetic torque at the level of $0.25T_{G\cdot n}$, $0.5T_{G\cdot n}$, and $T_{G\cdot n}$. According to (41), these torque values are provided based on the following values of the armature current projection i_{q0}: 10.5 A, 21.0 A, and 42.0 A. The calculation results are presented in Figure 12.

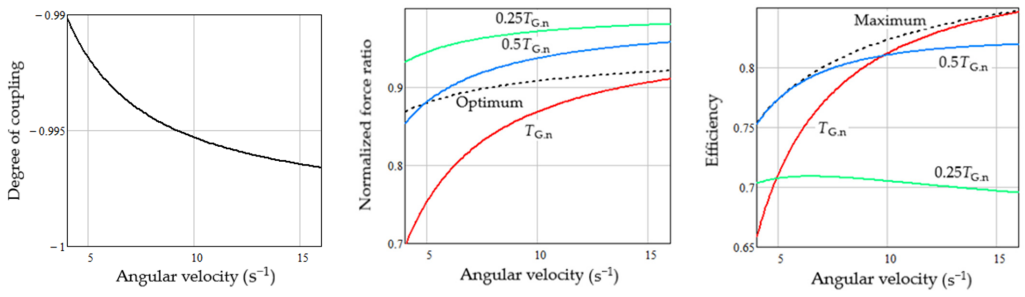

Figure 12. Dependences of the main parameters of the PMSG as the EC on its angular velocity: (**a**) degree of coupling, (**b**) reduced force ratio, (**c**) efficiency.

As can be seen from Figure 12a, as well as from the expression for q_G (51), the degree of coupling depends on the resistance ratio R_a/R_c and does not depend on the electrical load of the generator. According to (58), as the angular velocity of the latter increases, the resistance R_c increases as well, and therefore, q_G increases. According to (51), dependence $(Z\chi)_G$ is more complicated, and Figure 12b reflects this. According to the optimal dependence $(Z\chi)_{G.opt}(\omega)$ shown in Figure 12b with a dotted line, the maximum generator efficiency $\eta_G(\omega)$ possible for a specific value $q_G(\omega)$ is provided and shown in Figure 12c. However, with a change in the electrical load of the generator, as can be seen from Figure 12b, there are deviations $(Z\chi)_G$ in one direction and the other from the optimal value, which, respectively, leads to a decrease in $\eta_G(\omega)$, as can be seen from Figure 12c. From this figure, the highest efficiency values are obtained for $0.5T_{G.n}$, because for this torque of electrical load of the generator, the values of $(Z\chi)_G$ are as close as possible to the optimal values (Figure 12b). The lowest efficiency values are observed when the optimal values $(Z\chi)_G$ are exceeded, which can be seen from the curve for $0.25T_{G.n}$ and curves $\eta(Z\chi)$ shown in Figure 12c. It is worth noting that the biggest decrease in efficiency occurs due to the reduction in coupling and deviation from the optimal for this degree of the coupling operation point and not due to the amount of load.

5. Thermodynamic Analysis of Energy Conversion Efficiency in the "VAWT—PMSG" Complex

5.1. Thermodynamic Performance Indicators of the Studied PMSG Driven by the Studied VAWT

When the shaft of the studied VAWT (parameters in Table 1) is connected with the studied PMSG (parameters in Table 2), steady states of the WECS at wind speeds of 8 m/s, 10 m/s, and 12 m/s will be ensured by vector control of the generator armature current projections. Their dependences on the joint angular velocity of the VAWT and PMSG complex are shown in Figure 13.

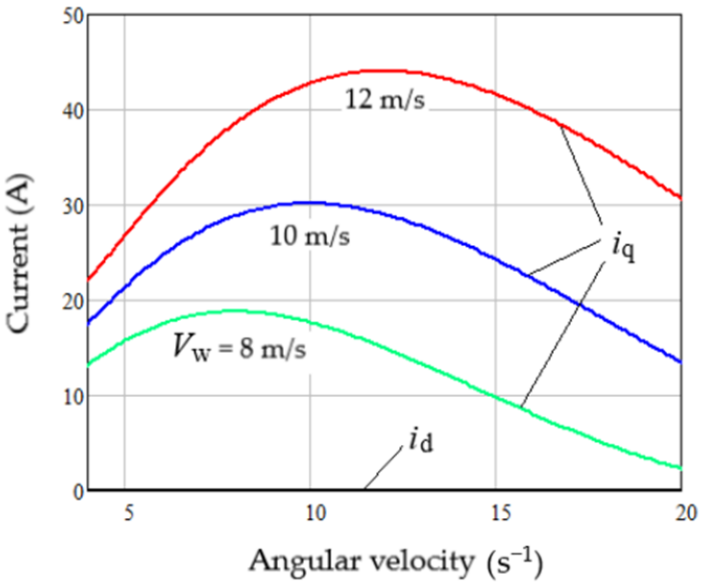

Figure 13. Dependencies of the PMSG armature current projections on the angular velocity of the VAWT with a generator at different values of the wind speed.

Under such conditions, the dependence $q_G(\omega)$ for the generator remains the same as shown in Figure 12a, and the dependences $(Z\chi)_G$ and $\eta_G(\omega)$, unlike those shown in Figure 12b,c, will have the form shown in Figure 14.

As can be seen from the obtained dependences, for every wind speed, there is a significant range of variation in the VAWT angular velocity with the PMSG, in which the generator efficiency is very close to the maximum possible. This is ensured by the fact that there is equality of $(Z\chi)_G = (Z\chi)_{G.opt}$ in the middle of these ranges (see Figure 14a).

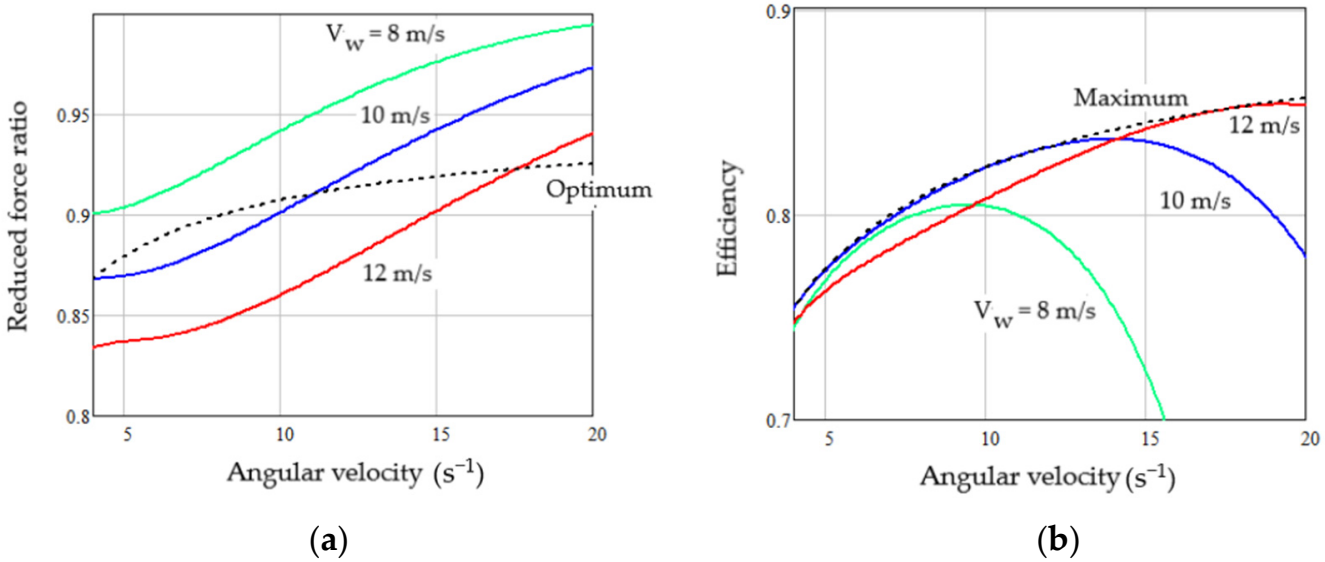

Figure 14. Dependencies of the reduced force ratio (**a**) and efficiency (**b**) of the PMSG driven by the studied VAWT on the angular velocity.

5.2. Thermodynamic Parameters of the WECS as a Cascade EC

The two ECs investigated above (VAWT and PMSG) are connected into one complex of WECSs in a cascade manner, as evidenced by the obtained linear systems of Equations (29) and (43), which describe the established operation mode of these EC components. In the following systems of equations, the necessary conditions for the cascade connection of the two investigated ECs are fulfilled: $X_1^o = X_2^i = \omega$, $J_1^o = J_2^i = T_{WT} = T_G$. The new complex EC obtained by the cascade connection of the two ECs studied above is characterized by several indicators. The dependence of these indicators on the angular velocity ω of the complex is shown in Figure 15.

From the point of view of the degree of coupling of the complex EC, which most affects the efficiency of the complex, the quality of the cascade connection is characterized by the connection coefficient γ. The dependences of $\gamma(\omega)$ on the angular velocity of the complex are calculated according to expression (20) for the three investigated wind speeds and are presented in Figure 15a. The same figure shows the dependences on the angular velocity of the optimal connection coefficients $\gamma_{opt}(\omega)$ of EC components calculated using Expression (21) for the same values of the wind speed. They are shown with specific dependences on the angular velocity of the complex of their degrees of coupling, which are shown, respectively, in Figures 9a and 12a. As can be seen from Figure 15a, the corresponding pairs $\gamma(\omega)$ and $\gamma_{opt}(\omega)$ for each of the wind speeds differ from each other but gradually approach each other as the angular velocity of the complex increases. This indicates the suboptimality of the cascade connection of the EC components into a complex, as can be seen from the dependences for the studied wind speeds of the degrees of coupling of the complex EC $q_\Sigma(\omega)$, calculated according to Expression (19), which are lower than the corresponding maximum possible values $q_{\Sigma.max}(\omega)$ calculated according to (22).

In addition to the degree of coupling of the complex EC, the efficiency of its operation is also affected by the operating mode point, which is characterized by the reduced force ratio of the complex $(Z\chi)_\Sigma$. Dependencies $(Z\chi)_\Sigma(\omega)$, calculated using expression (19) for the three investigated wind speeds, are shown in Figure 15c. This figure also shows the dependences on the angular velocity for the optimal values of the reduced force ratios of the complex $(Z\chi)_{\Sigma.opt}(\omega)$ corresponding to the optimal operating modes of the complex EC with the optimal connection coefficients $\gamma_{opt}(\omega)$ of the two components of the EC calculated using Expression (23) for the same values of the wind speeds. Since a source with free energy—VAWT powered by wind energy—is included at the input of the complex EC, it is advisable to take the maximum output power (15) as a criterion for the efficiency of

the complex EC. The optimal reduced force ratios for such an EC are calculated according to Expression (16) and are presented in Figure 15c based on the curves $(Z\chi)_{\Sigma.Pmax}(\omega)$. At the intersection points of the corresponding curves $(Z\chi)_{\Sigma}(\omega)$ and $(Z\chi)_{\Sigma.opt}(\omega)$ with $(Z\chi)_{\Sigma.Pmax}(\omega)$, the optimal values of the angular velocity ω_{opt} of the complex are obtained for the real and ideal connection of the two EC components, respectively.

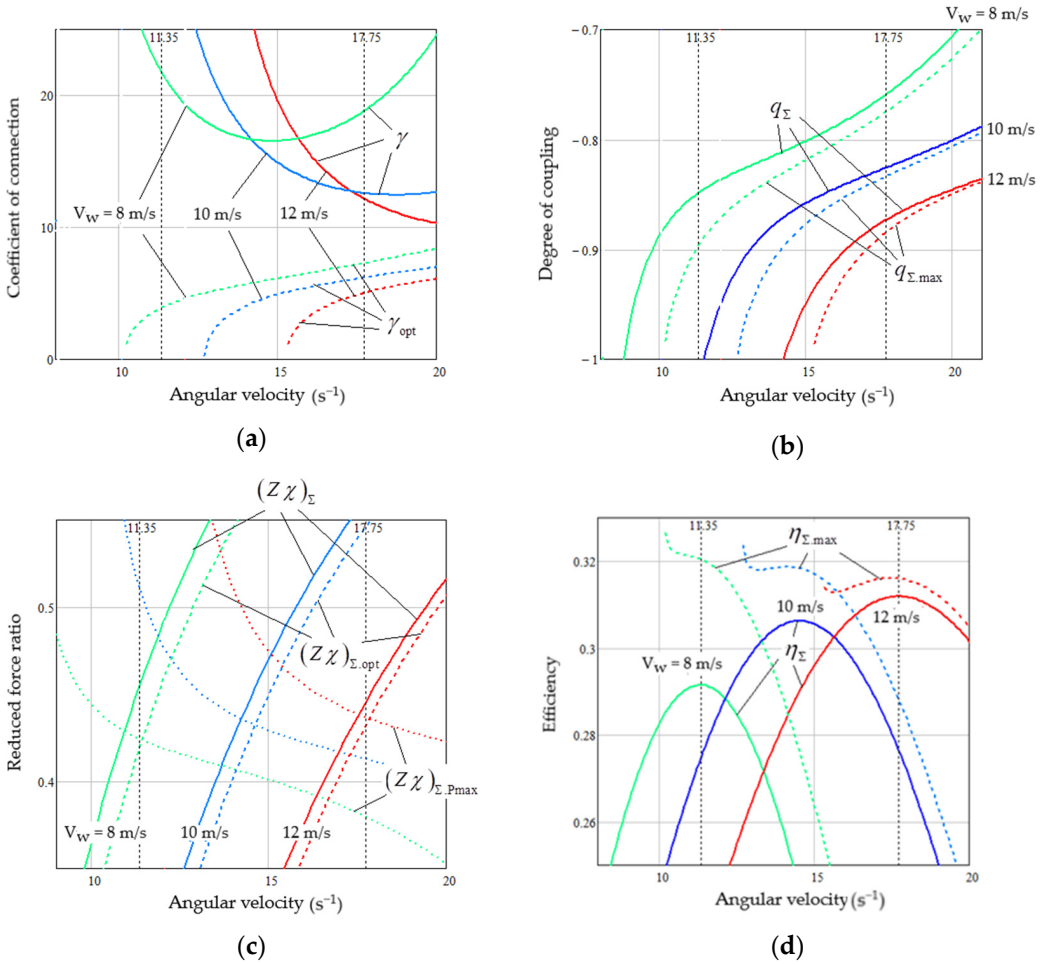

Figure 15. Dependencies of the main indicators of the experimental WECS as a cascade EC on the angular velocity of the VAWT with PMSG at different wind speeds: (**a**) the connection coefficient between two ECs, (**b**) total degree of coupling, (**c**) reduced force ratio, (**d**) efficiency.

Figure 15d shows the dependences of the wind power conversion efficiency $\eta_{\Sigma}(\omega)$ of the complex EC—the studied WECS—on the angular velocity of the complex at different wind speeds, calculated according to Expression (12) for the real obtained dependences $q_{\Sigma}(\omega)$ and $(Z\chi)_{\Sigma}(\omega)$. Since the power of the wind flow washing the wind rotor is constant for each of the wind speeds, the maximum values of the output power for each of the wind speeds are also provided at the maximum points of the curves $\eta_{\Sigma}(\omega)$. Also, Figure 15d shows the maximum possible efficiency dependencies on the angular velocity $\eta_{\Sigma,max}(\omega)$ of the complex at the studied wind speeds. They are calculated according to Expression (12) for the maximum values of the degree of coupling $q_{\Sigma.max}(\omega)$ and the optimal values of the reduced force ratios $(Z\chi)_{\Sigma.opt}(\omega)$ of the complex, corresponding to the optimal operating modes of the complex EC with optimal connection coefficients $\gamma_{opt}(\omega)$. As can be seen from the obtained dependences, the optimal combination of two components of the EC (VAWT and PMSG) provides a significant efficiency increase, especially at low wind speeds. Therefore, for V_w = 8 m/s, the efficiency can increase by 9.2%.

Figure 15d shows the optimal values of the angular velocity of the complex ω_{opt} for wind speeds of 8 m/s and 12 m/s to 11.35 s^{-1} and 17.75 s^{-1}, respectively (due to Mathcad

limitation of displaying only two markers on one axis). The same values of ω_{opt} are also shown in all other parts of Figure 15a–c. As can be seen from Figure 15c, at ω_{opt}, there is an intersection of the curves $(Z\chi)_{\Sigma.opt}(\omega)$ with the curves $(Z\chi)_{\Sigma.Pmax}(\omega)$, which, as mentioned above, corresponds to the ideal connection of the two components of the EC. For the intersection points of real curves $(Z\chi)_{\Sigma}(\omega)$ with curves $(Z\chi)_{\Sigma.Pmax}(\omega)$, the obtained values ω_{opt} are slightly higher, but these deviations are small.

5.3. Research on Ways to Improve the WECS Efficiency

The simulation results obtained in Sections 4 and 5 make it possible to determine the optimal operating points of the studied VAWT and PMSG, respectively, as well as the maximum performance indicators of their operation. The latter is conditioned by the given parameters of these devices: for the VAWT, by the characteristic $C_P(\lambda)$, and for the PMSG, by the relative losses in copper and steel (Table 2). However, having the cascade connection of the studied VAWT and PMSG, as shown by the results obtained in Section 5.2, the maximum values of the efficiency of the studied WECS are obtained as a compromise between the efficiencies of these devices. This is mainly due to the non-ideality of their cascade connection, which can be seen from the dependencies shown in Figure 15. At the same time, as can be seen from Figure 15d, there are reserves for improving the efficiency of the studied WECS. This paragraph explores ways of realizing these reserves.

For the connection coefficient γ, it can be seen from the Expression (20) that its deviation from the optimal value (21) depends on the ratio of its own kinetic coefficients—the output L_{oo} for VAWT and the input L_{ii} for PMSG—and this ratio is far greater than the optimal value γ_{opt} (Figure 15a).

As can be seen from (35), the value of L_{oo} for a VAWT with a given characteristic can be changed only by changing the turbine power. However, at the same time, the power of the generator increases respectively, from which the resistance of its armature winding is determined according to (54) and (41). Studies have shown that all of these changes lead to the invariance of the ratio between γ and γ_{opt} for the optimal VAWT angular velocities ω_{opt} at different wind speeds; however, ω_{opt} decreases with an increasing VAWT power. Therefore, the reserves for changing the parameters of the VAWT to optimize its connection with the PMSG remain only the choice of a WT with a different characteristic $C_P(\lambda)$, which can be the subject of a separate study.

Regarding the change in L_{ii} for the PMSG, as can be seen from (50), the following parameters of the generator can be variable: p, ψ_{pm}, R_a, R_{cn} та L_a. As research has shown, the values of R_a and R_{cn} at given relative power losses in copper and steel are completely dependent on p and ψ_{pm}, which are independent parameters of the PMSG. However, taking into account the dependencies (54) and (57), the changes in wide ranges of p and ψ_{pm} have absolutely no effect on the L_{ii} value obtained from (50) for the PMSG, which is easy to show analytically. The value of the inductance of the PMSG armature winding L_a, according to (56), also depends on the parameters p and ψ_{pm}. However, as shown above, this does not lead to a change in L_{ii}. Nevertheless, there is another independent parameter in (56)—the shift angle φ between the voltage and current vectors of the generator armature at its nominal angular velocity and nominal load. The conducted studies showed a significant influence of this parameter on the quality of the connection of the studied VAWT and PMSG, as can be seen in Figure 16. This shows how the maximum values of the overall efficiency of the studied WECS change depending on the set value of the nominal shift angle φ between the voltage and current vectors of the PMSG armature at different wind speeds (corresponding to the maximum of the curves shown in Figure 15d).

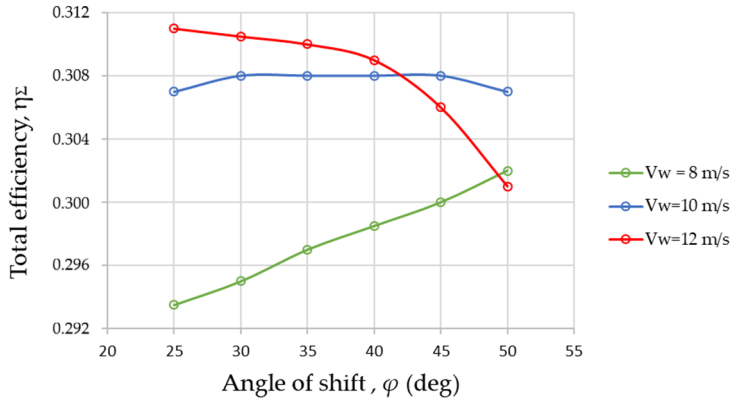

Figure 16. Dependencies of the overall efficiency of the studied WECS on the given value of the nominal shift angle φ between the voltage and current vectors of the PMSG armature at different wind speeds.

An analysis of the results shown in Figure 16 gives the possibility to choose the value $\varphi = 40°$ as an option for compromise. The dependences of the main indicators of the studied WECS obtained for this angle are shown in Figure 17. Based on Figure 17a, it can be said that at the optimal VAWT angular velocities for each of the studied wind speeds (which are slightly different from those obtained in Figure 15), the values of γ are closer to γ_{opt} than in Figure 15a. This ensures that the overall efficiency of the studied WECS is close to its maximum value (Figure 17b). It is almost perfect for $V_w = 12$ m/s, slightly worse for $V_w = 10$ m/s, and even worse for $V_w = 8$ m/s. However, it is a better option for the studied PMSG. An even closer option to the optimal one can be sought by taking a more complex type of PMSG, for example, with hybrid magnetoelectric and electromagnetic excitation [27], in which the parameters can be changed depending on the wind speed, which can be the subject of further research. To design such complex electromechanical systems, it is advisable to use modern approaches to realize digital and smart manufacturing, such as, for example, the digital twin [28].

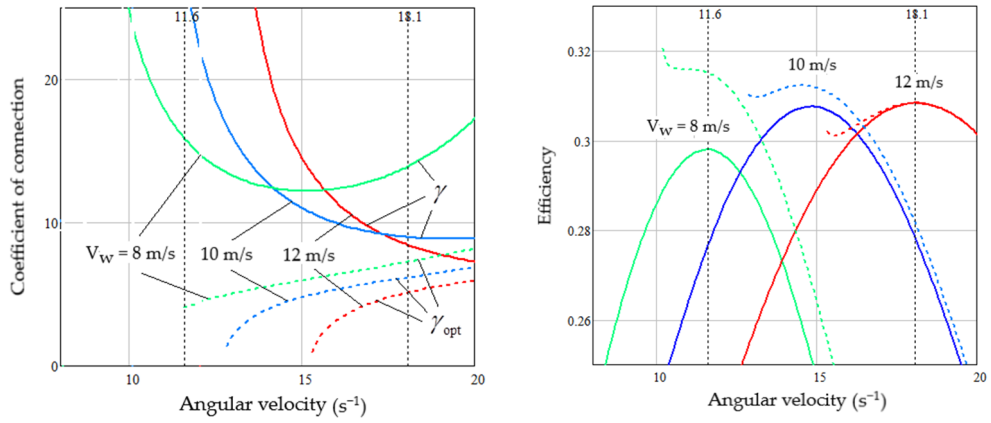

Figure 17. Dependencies of the main indicators of the studied WECS on the angular velocity of the VAWT—PMSG complex with the optimally chosen nominal value of the angle φ at different wind speeds: (**a**) the connection coefficient between two ECs, (**b**) efficiency.

6. Conclusions

The approach of linear non-equilibrium thermodynamics, in particular the method of the universal description of objects and subsystems as ECs, is promising for the analysis of energy processes and improving the efficiency of various systems, in particular renewable energy systems or energy storage systems. This approach makes it possible to assess the

energy quality of subsystems of different natures from one universal point of view without delving into the physical, chemical, or other features of the processes. Having a system of universal ECs, the next step can be taken—to identify the conditions for the best connection of such ECs. In this work, this is shown based on a specific example of applying the approach of linear non-equilibrium thermodynamics to the analysis of the efficiency of energy conversion in the WECS, which consists of two devices connected in cascade—the VAWT and the vector-controlled PMSG. To the best of the author's knowledge, this is the first time that the VAWT and PMSG have been mathematically characterized as linear ECs, enabling their linearization at operating points within a specified range of common angular velocities. By further applying the universal description of these ECs using a system of dimensionless parameters and characteristics, it became possible to obtain the degrees of coupling between the input and output of these devices, choose the parameters for their optimal operating points based on specific criteria (corresponding to the maximum output power and the maximum efficiency), and evaluate their efficiency indicators. The obtained models of the VAWT and PMSG, as linearized ECs, will be used in the future to study other power-generating complexes.

The method of the universal description of ECs has been further developed to assess the patterns of cascade connections between two ECs. This advancement allows for a determination of the quality indicator of a specific connection and its impact on the performance indicators of the resulting equivalent cascaded EC. An analysis of the connection quality of the studied VAWT and PMSG showed that there are reserves in increasing the efficiency of the studied WECS built on their basis. The conducted research made it possible to identify which of the VAWT and the PMSG parameters have an impact on the energy quality of their connection. In particular, the effective factor affecting the quality of this connection turned out to be the angle of shift between the voltage and current vectors of the generator in the nominal mode. This study made it possible to substantiate the optimal value of this angle, equal to 40°. This value provides the best approximation to the optimal connection of the investigated ECs in the entire range of wind speeds, especially with medium and high winds.

Author Contributions: Conceptualization, I.S. and M.L.; methodology, I.S. and Y.B.; software, I.S. and Y.B.; validation, M.L.; formal analysis, I.S. and M.L.; investigation, I.S. and Y.B.; resources, I.S.; data curation, Y.B.; writing—original draft preparation, I.S. and Y.B.; writing—review and editing, I.S. and M.L.; visualization, Y.B.; supervision, I.S. and M.L.; project administration, I.S. and M.L.; funding acquisition, M.L. All authors have read and agreed to the published version of the manuscript.

Funding: This research received no external funding.

Data Availability Statement: Not applicable.

Conflicts of Interest: The authors declare no conflict of interest.

References

1. Turns, S.R.; Pauley, L.L. *Thermodynamics: Concepts and Applications*, 2nd ed.; Cambridge University Press: Cambridge, UK, 2020; 854p.
2. Demirel, Y. *Non-Equilibrium Thermodynamics: Transport and Rate Processes in Physical, Chemical and Biological Systems*, 2nd ed.; Elsevier Science & Technology Books: Amsterdam, The Netherlands, 2007; 754p.
3. Christen, T. *Efficiency and Power in Energy Conversion and Storage: Basic Physical Concepts*; CRC Press, Taylor & Francis Group: Boca Raton, FL, USA, 2018; 178p. [CrossRef]
4. Kleidon, A. Working at the Limit: A Review of Thermodynamics and Optimality of the Earth System. *Earth Syst. Dyn. Discuss.* **2022**, preprint. [CrossRef]
5. Perera, S.M.H.D.; Putrus, G.; Conlon, M.; Narayana, M.; Sunderland, K. Wind energy harvesting and conversion systems: A technical review. *Energies* **2022**, *15*, 9299. [CrossRef]
6. Shchur, I.; Klymko, V.; Xie, S.; Schmidt, D. Design features and numerical investigation of counter-rotating VAWT with co-axial rotors displaced from each other along the axis of rotation. *Energies* **2023**, *16*, 4493. [CrossRef]
7. Wu, C.; Wang, Q.; Yuan, R.; Luo, K.; Fan, J. Large eddy simulation of the layout effects on wind farm performance coupling with wind turbine control strategies. *ASME. J. Energy Resour. Technol.* **2022**, *144*, 051304. [CrossRef]

8. Wang, Q.; Luo, K.; Wu, C.; Tan, J.; He, R.; Ye, S.; Fan, J. Inter-farm cluster interaction of the operational and planned offshore wind power base. *J. Clean. Prod.* **2023**, *396*, 136529. [CrossRef]
9. Zhang, S.; Luo, K.; Yuan, R.; Wang, Q.; Wang, J.; Zhang, L.; Fan, J. Influences of operating parameters on the aerodynamics and aeroacoustics of a horizontal-axis wind turbine. *Energy* **2018**, *160*, 597–611. [CrossRef]
10. Sahin, A.D.; Dincer, I.; Rosen, M.A. Thermodynamic analysis of wind energy. *Int. J. Energy Res.* **2006**, *30*, 553–566. [CrossRef]
11. Hu, W.; Liu, Z.; Tan, J. Thermodynamic analysis of wind energy systems. In *Wind Solar Hybrid Renewable Energy System*; Kenneth, O.E., Tahour, A., Aissaou, A.G., Eds.; IntechOpen: London, UK, 2019; pp. 1–19. [CrossRef]
12. Diyoke, C.; Ngwaka, U. Thermodynamic analysis of a hybrid wind turbine and biomass gasifier for energy supply in a rural off-grid region of Nigeria. *Energy Sources Part A Recovery Util. Environ. Eff.* **2021**, 1–26. [CrossRef]
13. Zhang, Y.; Yang, K.; Li, X.; Xu, J. Thermodynamic analysis of energy conversion and transfer in hybrid system consisting of wind turbine and advanced adiabatic compressed air energy storage. *Energy* **2014**, *77*, 460–477. [CrossRef]
14. Koschwitz, P.; Bellotti, D.; Sanz, M.C.; Alcaide-Moreno, A.; Liang, C.; Epple, B. Dynamic parameter simulations for a novel small-scale power-to-ammoniac. *Processes* **2023**, *11*, 680. [CrossRef]
15. Zhang, Y.; Lin, Y.; Lin, F.; Yang, K. Thermodynamic analysis of a novel combined cooling, heating, and power system consisting of wind energy and transcritical compressed CO_2 energy storage. *Energy Convers. Manag.* **2022**, *260*, 115609. [CrossRef]
16. Ehyaei, M.A.; Baloochzadeh, S.; Ahmadi, A.; Abanades, S. Energy, exergy, economic, exergoenvironmental, and environmental analyses of a multigeneration system to produce electricity, cooling, potable water, hydrogen and sodium-hypochlorite. *Desalination* **2021**, *501*, 114902. [CrossRef]
17. Vosough, A.; Vosough, S. Different kind of renewable energy and exergy concept. *Int. J. Multidiscip. Sci. Eng.* **2011**, *2*, 1–7.
18. Westerhoff, H.V.; van Dam, K. *Thermodynamics and Control of Biological Free-Energy Transduction*; Elsevier: Amsterdam, The Netherlands, 1987; 298p. [CrossRef]
19. Shchur, I.; Rusek, A.; Lis, M. Optimal frequency control of the induction electric drive based on the thermodynamics of irreversible processes. *Electrotech. Comput. Syst.* **2011**, *3*, 377–380. Available online: https://eltecs.op.edu.ua/index.php/journal/article/view/751 (accessed on 17 February 2019).
20. Kondepudi, D.; Prigogine, I. *Modern Thermodynamics: From Heat Engines to Dissipative Structures*, 2nd ed.; John Wiley & Sons: New York, NY, USA, 2015; 560p. [CrossRef]
21. Li, Y.; Yang, S.; Feng, F.; Tagawa, K. A review on numerical simulation based on CFD technology of aerodynamic characteristics of straight-bladed vertical axis wind turbines. *Energy Rep.* **2023**, *9*, 4360–4379. [CrossRef]
22. Krause, P.; Wasynczuk, O.; Sudhoff, S.; Pekarek, S. *Analysis of Electric Machinery and Drive Systems*, 3rd ed.; Wiley: Hoboken, NJ, USA, 2013; 688p. [CrossRef]
23. Majout, B.; El Alami, H.; Salime, H.; Zine Laabidine, N.; El Mourabit, Y.; Motahhir, S.; Bouderbala, M.; Karim, M.; Bossoufi, B. A review on popular control applications in wind energy conversion system based on permanent magnet generator PMSG. *Energies* **2022**, *15*, 6238. [CrossRef]
24. Shchur, I.; Rusek, A.; Biletskyi, Y. Energy-shaping optimal load control of PMSG in a stand-alone wind turbine as a port-controlled Hamiltonian system. *Przegląd Elektrotechniczny (Electr. Rev.)* **2014**, *5*, 50–55. [CrossRef]
25. Torki, W.; Grouz, F.; Sbita, L. Vector control of a PMSG direct-drive wind turbine. In Proceedings of the 2017 International Conference on Green Energy Conversion Systems (GECS), Hammamet, Tunisia, 23–25 March 2017; pp. 1–6. [CrossRef]
26. Fernandez-Bernal, F.; García-Cerrada, A.; Faure, R. Determination of parameters in interior permanent-magnet synchronous motors with iron losses without torque measurement. *IEEE Trans. Ind. Appl.* **2001**, *37*, 1265–1272. [CrossRef]
27. Golovko, V.M.; Ostroverkhov, M.Y.; Kovalenko, M.A.; Kovalenko, I.Y.; Tsyplenkov, D.V. Mathematical simulation of autonomous wind electric installation with magnetoelectric generator. *Nauk. Visnyk Natsionalnoho Hirnychoho Universytetu* **2022**, *5*, 74–79. [CrossRef]
28. Liu, L.; Guo, Y.; Yin, W.; Lei, G.; Zhu, J. Design and optimization technologies of permanent magnet machines and drive systems based on digital twin model. *Energies* **2022**, *15*, 6186. [CrossRef]